Batteries & Supercaps

Research Article
doi.org/10.1002/batt.202400386

Chemistry Europe
European Chemical Societies Publishing

www.batteries-supercaps.org

Thermal Runaway of Na-Ion Batteries with $Na_3V_2O_2(PO_4)_2F$ Cathodes

Tatiana K. Zakharchenko,*[a, b] Dmitriy I. Nikiforov,[a] Georgiy D. Serdyukov,[a] Pavel V. Komissarov,[a] Mikhail O. Shkuratov,[a, b] Alexander V. Dzuban,[b] Grigorii P. Lakienko,[b] Yuriy A. Gordienko,[a] Lada V. Yashina,[a, b] and Daniil M. Itkis[a, c]

The metal-ion battery manufacturing growth rates increase attention to the safety issues. For promising sodium-ion batteries, this topic has been studied in much less detail than for the lithium-ion ones. Here, we explored the thermal runaway process of Na-ion pouch cells with the $Na_3V_2O_2(PO_4)_2F$ (NVOPF)-based cathode. The thermal runaway onset temperature for such cells is noticeably higher than that for the NMC-based LIBs. We show that thermal runaway is triggered by the anode and the separator decomposition rather than by the processes at the cathode. The composition of the gas mixture released during thermal runaway process is similar to that for Li-ion batteries. The results suggest that sodium-ion batteries based on polyanionic cathodes can pave the way to safer metal-ion energy storage technologies.

Introduction

The transfer from fossil fuels to renewable energy sources implicates extensive use of electrochemical storage systems, specifically, metal-ion batteries. Next decade, the growing electric vehicle market will provoke a significant increase in lithium-ion batteries (LIBs) demand.[1,2] It is well recognized that devices containing such rechargeable batteries could pose potential threat since a cell could ignite during operation. For this reason, recently much attention has been paid to the safety issues of various batteries, primarily lithium-ion ones. Many authors have focused on the effects of thermal, mechanical, and electrical abuse on the thermal runaway process.[3–7]

It is well known that batteries with layered oxide cathode materials such as $Li[Ni_xCo_xMn_x]O_2$ (NMC), $LiCoO_2$, and $Li[Ni_xCo_yAL_z]O_2$ are generally less safe than those with $LiFePO_4$ (LFP) cathodes. The layered oxide materials decompose at lower temperatures[8–10] with oxygen release that intensifies the thermal runaway (TR) process.[11,12] For instance, the maximum temperature observed in Ref.[13] for NMC cells during TR reaches 1000 °C, while for LFP it is about 400 °C. This trend is confirmed further in Refs.[14,15] Also, TR for LFP-based cells occurs at a higher temperature of the cell surface.[16–18] At the same time, the authors of Ref.[19] found a direct correlation between the total enthalpy of the TR and the cell capacity, regardless of the cathode material used. The TR process is also strongly influenced by the battery state of charge (SoC).[20]

Together with the lithium-ion batteries, sodium-ion cells are now in focus of scientific interest[21–24] due to higher abundance of sodium in the Earth's crust and lower cost compared to lithium. At the same time, sodium-ion batteries (SIBs) have lower specific characteristics so they are considered as a solution for medium- to large-scale stationary energy storage applications.[25] At such a scale, safety plays a key role; however, so far for sodium batteries the TR process has not been comprehensively studied. A limited number of papers on this topic has been recently published,[26–36] with most of them being devoted to batteries with the layered oxide cathode materials.[27,29,30,32,35,36] These studies pinpoint although the thermal stability of sodium layered oxide materials is generally worse than that of their lithium analogues,[8] TR for layered oxide SIBs does not occur during standard safety tests (nail penetration, overcharge, internal short circuit, heating to 150 °C, etc).[30,32] Cylindrical 18650 cells based on $Na_3V_2(PO_4)_2F_3$ (NVPF) also do not demonstrate TR under different abuse conditions[31] including heating up to 135 °C. However, another study[26] employing the 18650 Tiamat NVPF-based cells demonstrated that TR readily occurs upon heating to 120–140 °C. Unfortunately, there is a lack of TR data regarding other types of promising SIBs with fluorophosphate-based cathode.[37] At the same time, in comparison with other cathode materials, polyanionic compounds provide relatively stable cycling performance, high working voltage, superior thermal stability, and remarkable safety.[38] In particular, in Ref.[8] it was shown that charged polyanionic Na-ion cathode materials ($Na_3V_2(PO_4)_3$, β-$NaVP_2O_7$) are more thermally stable than charged layered oxide $NaNi_{1/3}Fe_{1/3}Mn_{1/3}O_2$. Therefore, a Na-ion battery with polyanionic compounds should be safer than that with a layered oxide.

Here, we focus on the TR process of fully charged sodium-ion pouch cells with a $Na_3V_2O_2(PO_4)_2F$ (NVOPF) – based positive electrode. We triggered the TR by external heating. We further compared the TR of lithium NMC-based cells versus NVOPF-

[a] T. K. Zakharchenko, D. I. Nikiforov, G. D. Serdyukov, P. V. Komissarov, M. O. Shkuratov, Y. A. Gordienko, L. V. Yashina, D. M. Itkis
N.N. Semenov Federal Research Center for Chemical Physics, Kosygina Street 4, 119991 Moscow, Russia
E-mail: t.zakharchenko@chph.ras.ru

[b] T. K. Zakharchenko, M. O. Shkuratov, A. V. Dzuban, G. P. Lakienko, L. V. Yashina
Lomonosov Moscow State University, Leninskie gory 1 bld. 3, 119991 Moscow, Russia

[c] D. M. Itkis
Moscow Center for Advanced Studies, Kulakova str. 20, 123592 Moscow, Russia

Research Article
doi.org/10.1002/batt.202400386
Chemistry Europe
European Chemical Societies Publishing

based sodium-ion pouch cells. To uncover the key triggering factors of the TR, we measured the DSC curves for individual Na-ion cell components. The composition analysis of the gases released after the TR was also carried out.

Experimental Section

Thermal Runaway Studies

Pouch Cells

NMC-based Li-ion cells LP304560 (Robiton) were used in this study. Before the experiments, the protection circuit boards were removed to ensure more accurate electrochemical measurements. The cell characteristics declared by the manufacturer were: nominal capacity of 700 mAh at C/2, nominal voltage of 3.7 V. The cell dimensions were 60×45×3 mm (L×W×H). For the TR studies, all cells were charged to 100% SoC (CC charge to 4.2 V at 100 mA; after CC stage the cell voltage relaxed for 10 min and then the cell was charged up back to 4.2 V; such top up cycle was repeated 20 times).

Sodium-ion pouch cells were fabricated in-house. These cells comprised a Z-folded stack of 5×5 cm^2 double-side coated electrodes (5 or 10 electrode pairs) with a Celgard 2325 trilayer polypropylene/polyethylene/polypropylene separator in between. The electrodes were produced by coating the aluminium foil. Its thickness was 400 μm for anode. For cathode it was 580 μm and 450 μm for 5 and 10 electrode pairs, respectively. The slurries were prepared by mixing the active material (hard carbon (HC) and NVOPF were synthesized using the techniques reported in Ref.[39] and Ref.,[40] respectively. A polymer binder PVdF (Solef 5130, Solvay), carbon black (Super P, Timcal), and carbon nanotubes (Tuball, OCSiAl) were mixed in N-methyl-2-pyrrolidone. For the cathode and anode slurries the solid components ratios were 92:1.5:6:0.5 and 93:1.5:5:0.5, respectively. The areal capacity of the electrodes was about 2 mAh/cm^2. 1 M solution of $NaPF_6$ in ethylene carbonate (EC): diethyl carbonate (DEC) 1:1 (wt.) with an addition of 1% fluoroethylene carbonate (Kishida Chemicals) was used as the electrolyte. The cell capacity was measured at the 5th charge-discharge cycle at 0.1 C and comprised 294 mAh and 850 mAh, respectively. The energy density of last one is 106 Wh h/kg. The electrochemical data can be found in Figure S1 in Supplementary materials. Before the TR, Na-ion pouch cells were charged similar to the NMC-based Li-ion cells to standardize the TR experimental conditions.

Experimental Setup for the TR Studies

The experimental setup scheme is presented in Figure 1a. It consists of a sealed steel chamber (Figure 1b) connected to a gas system. The chamber has a removable sliding cover for cell loading. The lid and the chamber are sealed with a Teflon ring gasket allowing to keep the TR products at elevated pressure until they are cooled down completely. The thermocouple wire and power cables for the heating elements are fed through the sealed glands on the lid.

The setup is equipped with a gas control and collection system that enable evacuating the sample gas cylinder, sampling the TR gaseous products and their removal from the setup after the experiment. The agas system includes a manifold with valves, a 1 liter sample cylinder, an overpressure sensor (Oven PD100I-DI0.6-113-0.25-R), a vacuum pump, and a compressor for the system venting. The overpressure sensors are connected to the system in the vicinity of the sampling cylinder to avoid high temperatures of the gas media.

For the TR experiments, the cell under study was fixed inside the chamber between two resistive heating plates (90×90 mm^2, 250 W maximum power, Normat) (Figure 1c). The heat flow was transferred from the heater to the cells *via* round shaped plates of polished copper (22 mm in diameter, 2 mm thickness (marked as "heat transfer interface" in Figure 1a). The plates were installed symmetrically on both sides of the cell. The assembly of the cell and the heating plates was wrapped in fiberglass tissue to minimize the heat loss due to convection. The heating ramp was driven by a PID controller (Thermodat 19E6) with temperature feedback from thermocouples installed in the heaters. Cold junction temperature correction was carried out using semiconductor temperature sensors integrated into the temperature controller. The heating rate was 5 °C/min.

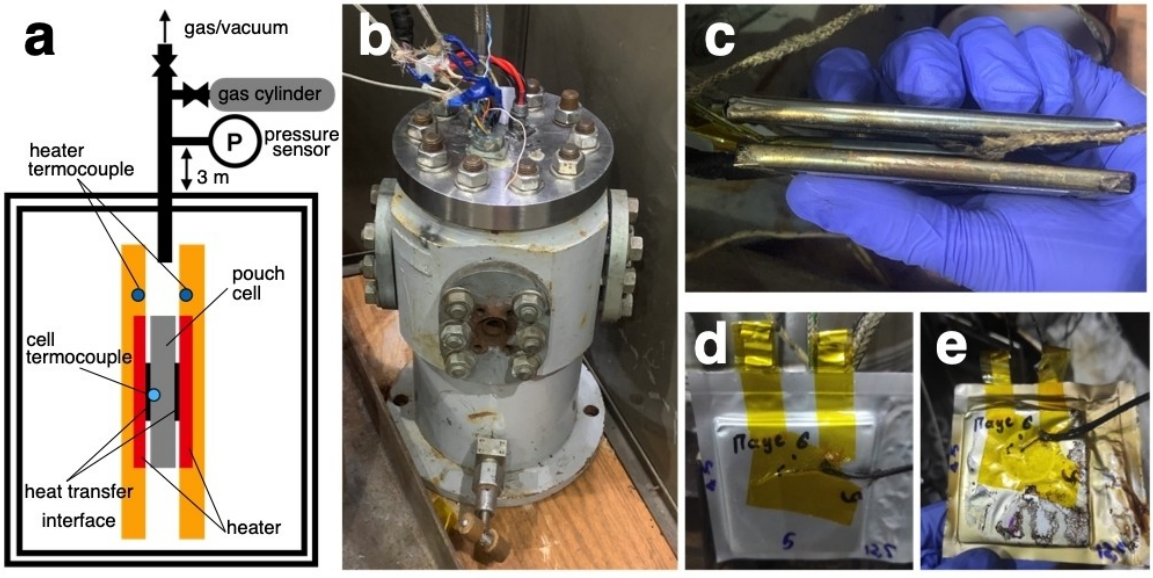

Figure 1. General scheme of the setup for TR studies (a). Photos of the experimental chamber (b), a cell with mounted heaters (c) and Na-ion pouch cell before (d) and after the heating (e).

Research Article
doi.org/10.1002/batt.202400386
Chemistry Europe
European Chemical Societies Publishing

Gas Chromatography

For the gas analysis, a Crystal 2000 chromatograph (Chromatek) was used. To separate the gas mixture, columns filled with zeolite (5 Å) and Porapak Q sorbent were used. The zeolite-packed column was used to analyze permanent gases and methane. Argon was used as a carrier gas. The Porapak Q column was used to analyze hydrocarbons with helium as a carrier. The columns with the adsorbents were maintained at 80 °C using a thermostat. The gas samples were injected from the sample cylinder through evaporators at 150 °C. From the columns, the gas was supplied to a thermal conductivity detector heated to 160 °C.

DSC Measurements

Materials Preparation

The slurries used for further electrode fabrication were prepared by mixing 93 wt.% active material (HC and NVOPF, same as for pouch cells), 5 wt. % polymer binder PVdF (Kynar), 1.5 wt. % carbon black (Super P, Timcal), and 0.5 wt. % carbon nanotubes (Tuball, OCSiAl) in N-methyl-2-pyrrolidone (Lukshim). Subsequently, the slurries were spread on Al foil and dried overnight. Electrodes were rolled and punched into 15 mm discs and dried overnight under vacuum at 120 °C for HC and at 60–70 °C for NVOPF. The synthesis of sodium ethylene dicarbonate (SEDC) was performed according to Ref.[41] Details are provided in the Supporting information.

Electrochemical Measurements

The galvanostatic charge/discharge experiments were performed in Swagelok-type cells built in-house. HC or NVOPF were used as working electrodes, metallic sodium (Komponent reactiv) as a counter electrode. The electrodes were separated by a glass fiber membrane (Whatman GF/A) wetted by 100–150 μL of 1 M $NaPF_6$ solution (98 %, Sigma, dried before use under vacuum for 2 days at 30 °C) in a 1 : 1 (wt.) mixture of EC (99 %, anhydrous, Sigma) and DEC (Gelon). Cells were assembled in an Ar-filled glovebox (VBOX PRO, Vilitek) with less than 0.1 ppm humidity and about 10 ppm of oxygen. Galvanostatic cycling was performed using a Biologic SAS MPG-2 battery cycler.

The HC cells were cycled 10 times between 2 and 0.01 V at 28 mA/g specific current. For full sodiation, the cells were additionally charged at 7 mA/g–0.01 V and held at 0.01 V with 1.75 mA/g current cut-off. For complete desodiation, the cells were discharged to 4.2 V at 28 mA/g; after the CC stage the cell voltage was allowed to relax for 30 min; then the cell was charged up back to 4.2 V. Such a top-up cycle was repeated 10 times.

The NVOPF-based cells were charged to 4.3 V at 13 mA/g specific current.

Materials Testing

Thermal analysis was carried out using DSC 204 HP Phoenix® and DSC 200 F3 Maia differential scanning calorimeters (NETZSCH, Selb, Germany) at ambient pressure. The instruments were pre-calibrated for temperatures and enthalpies of phase transitions of pure (99.99 + %) standard substances in compliance with the ASTM Practices E 967 and E 968: H_2O, benzoic acid, In, Sn, Bi, Pb, Zn. RMSD for temperature and heat effect determination were 0.2 °C and 5 %, respectively. The experimental data were processed with the NETZSCH Proteus® Software according to ASTM E 794 and ISO 11357–1.

Samples were prepared as follows. The cells were disassembled inside the Ar-filled glovebox, then the electrode coatings were scratched from the Al foils and loaded as is into aluminium crucibles, which were immediately sealed to prevent any air contact prior to the DSC measurements. Some samples were studied without the electrolyte. To remove the electrolyte, after the cell disassembly the electrodes were soaked in 1 mL of DEC for 20–30 min and consequently dried under vacuum for 20–30 min. Crucibles for model DSC experiments with SEDC, Na metal-electrolyte mixture, and a Celgard 2325 separator were prepared similar to the electrodes. The sample mass was determined from the difference between empty and filled crucibles using A&D GH-202 analytical balance.

Samples weighing 1.00–10.00 mg were ramped from 10–450 °C with a heating rate of 5 °C/min under argon (99.993 %) flow of 30 mL/min in alumina crucibles with pierced lids. The hole in the lid was made at the same time as the crucible was placed in the DSC measurement system purged with argon to avoid any air exposure.

Results and Discussion

The heating curves of TR experiments for the Li-ion (NMC) and Na-ion ($Na_3V_2O_2(PO_4)_2F$) cathode and HC anode) pouch cells are shown in Figure 2. The TR onset temperatures for the cell for NVOPF cathode materials is 194 °C; it noticeably exceeds the

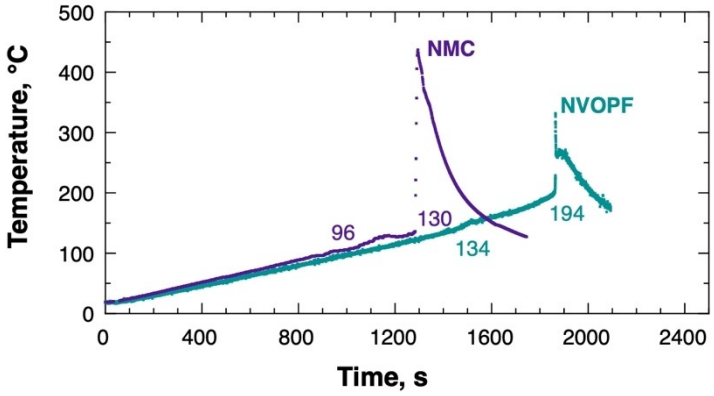

Figure 2. Temperature profiles of charged Li-ion pouch cell with the NMC cathode (700 mAh) and Na-ion pouch cell with the NVOPF cathode (850 mAh). The heating rate is 5 °C/min.

Research Article
doi.org/10.1002/batt.202400386
Chemistry Europe
European Chemical Societies Publishing

value for the oxide-based cell (130 °C), since it is known that the phosphate LFP-based batteries are more thermally stable than those with the NMC cathodes.[13,14,17] Alongside with the TR onset temperature, the maximum temperature reached is an important safety parameter. For the NVOPF-based cell, the maximal temperature is only 327 °C, which is lower than that for the NMC-based one (443 °C). Moreover, the NVOPF pouch cell case (see Figure 1d and e) was not destroyed after the TR in contrast to the NMC LIB (Figure S3).

Similar to the TR onset, the self-heating onset temperature of the NVOPF-based SIB is 134 °C, which is again higher than that for the NMC-based pouch LIB (102 °C). It should be noted that for both cells the self-heating begins simultaneously with the cell venting (see Figure S4a and S5).

Next, we studied the processes occurring in NVOPF-based cells upon heating in more detail. For this purpose, sodiated and desodiated HC samples and desodiated NVOPF were investigated using DSC. The cells with HC working electrodes were fully charged and discharged (to 0.01 and 2 V, respectively). The NVOPF electrodes were desodiated in the cells by charging to 4.3 V. The corresponding electrochemical curves are shown in the Supporting Information (Figure S6–S8). Figure 3 illustrates the relationship between the SIB behavior during the TR experiment with the thermoanalytic data for the individual cell components. Figure 3a exhibits the cell temperature and voltage *vs.* the heater temperature for comparison with the DSC data.

The self-heating onset for LIBs is normally associated with the SEI decomposition.[6] We analyzed the thermal decomposition of the anode material in SIBs using cycled anode materials, a mixture of electrolyte, and sodium metal. Also, we studied sodium ethylene decarbonate (SEDC) that is assumed to be the main component of SEI similar to the lithium system.[41,42] The curve shape in Figure 3b for fully sodiated HC is typical for the DSC experiments reported in literature.[8,43,44] However, the absolute temperature value in our work is a bit lower than the previously reported data. For the sodiated HC, we observed heat release starting at *ca.* 65 °C (detailed description of all thermal effects is presented in the Supporting information). We observed the SEDC decomposition at a similar temperature.

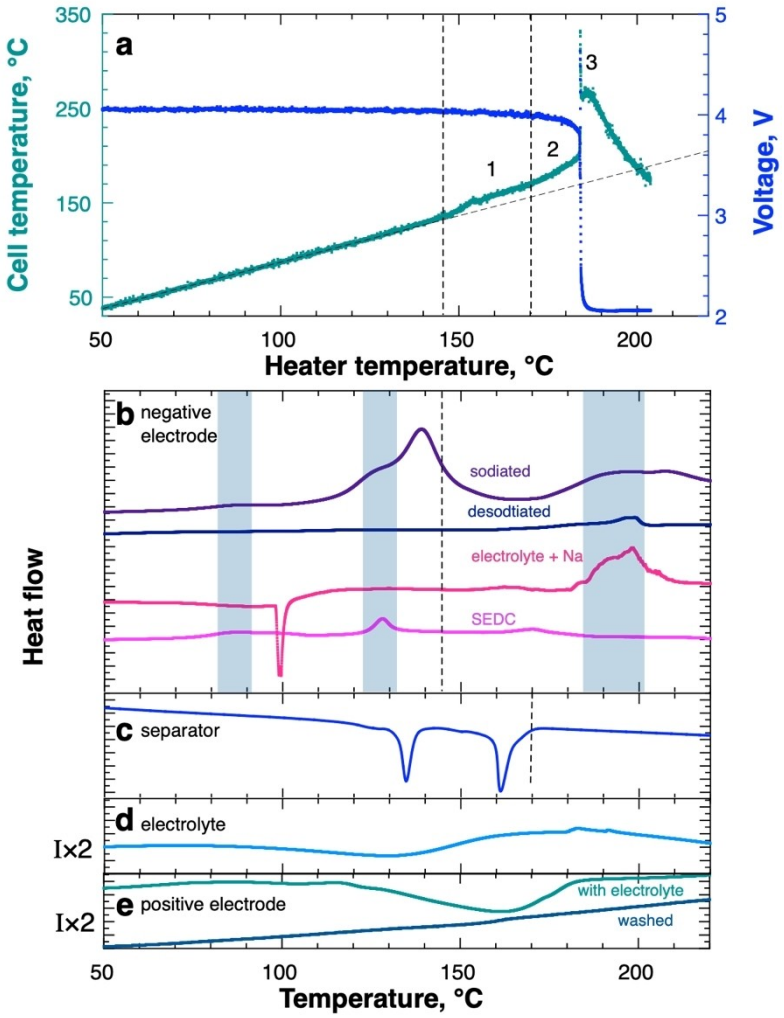

Figure 3. Cell temperature and voltage vs heater temperature for the 850 mAh Na-ion pouch cell (a). DSC profiles for sodiated and desodiated HC negative electrode, a mixture of metallic Na and the electrolyte (1 M $NaPF_6$ in EC/DEC (1 : 1 by weight)) and sodium ethylene dicarbonate (b); the separator (c); the electrolyte (d); washed and unwashed charged NVOPF electrode (e).

Research Article
doi.org/10.1002/batt.202400386
Chemistry Europe
European Chemical Societies Publishing

Further, a more intense exothermic process at the anode material and SEDC starts at a 100 °C and 115 °C, respectively. From the electrochemical data (see Figure S7 in the Supporting information), we can estimate the SEDC mass as only *ca.* 10% of the total mass of the charged electrode sample. The amount of heat generated around the peak at 139 °C for the sodiated HC electrode is, however, higher by more than an order of magnitude than for pure SEDC (with a peak at *ca.* 128 °C). We believe that the major contribution to heat release for sodiated HC can be ascribed to a secondary reaction of the electrolyte with the bare anode material (as the primary SEI decomposed earlier, between 100 and 130 °C). We assume that these processes are the main cause for the initial SIB self-heating (stage 1) starting around 145 °C. The slightly higher SIB self-heating onset temperature can be explained by the difference between the temperature at the pouch cell surface and that at the electrodes inside of the cell, as well as by the consequent delay required for the heat transfer.

The intensification of the self-heating (stage 2) is associated with the separator as the polypropylene layer melts at ~160 °C, according to the DSC data (Figure 3c) and the literature[45,46] (the first peak at ~135 °C corresponds to polyethylene layer melting).[47,48] During this stage, a cell voltage decrease is also observed. At the last stage (stage 3), an internal short circuit occurs, accompanied by the voltage drop, Joule heating, and the TR. Above 180 °C, self-heating is also promoted by the reaction of the electrolyte with sodium, which can be stored in HC as metal clusters in the micropores.[49] Similar heat release can be observed for the reaction of metallic sodium with the electrolyte (Figure 3b). It is worth noting that, in contrast to the LFP-based cell,[50] reactions of NVOPF with a carbonate-based electrolyte, according to our data, are endothermic (Figure 3e). The only study of the desodiated NVOPF thermal stability reports that the exothermic effect during heating of the washed electrode is weak and is extended along the temperature axis,[8] which is in line with our observations. For the NVOPF with the electrolyte, a noticeable endothermic effect is observed above 120 °C (the total heat absorption is four times less than that released during the decomposition of anode materials), which agrees with the data in Ref.[51] where a similar material, oxygen-doped NVPF, was studied. It should be noted that this process occurs at a higher temperature than the electrolyte evaporation (Figure 3d) and, therefore, we suppose that it is not directly related to it. A detailed study of the abnormal behavior of the cathode material is beyond the scope of this work.

The thermal runaway takes place when the heat generation rate exceeds the heat dissipation rate,[52] therefore the onset temperature depends strongly on the mass and geometry of the cells. We compared thermal behavior of SIBs with a different number of positive and negative electrode couples and thus different thickness. As indicated in Figure S4, typical temperature onsets for self-heating seem to be the same for the cells under comparison. However, as the heat dissipation rate is nearly the same (only the thickness varied since the 294 and 850 mAh cells include 5 and 10 electrode pairs, respectively) and the heat generation is lower for the smaller SIB, we did not observe a sharp temperature rise for the latter sample.

The gases released during the thermal runaway of a Na-ion cell were studied by gas chromatography. The results are presented in Figure 4. Two columns filled with zeolite (5 Å) and Porapak Q sorbent were used for the analysis of permanent gases and hydrocarbons, respectively. The corresponding chromatograms are plotted in Figure 4a and b.

The gas composition except for nitrogen and oxygen (as the thermal runaway experiment was carried out in air) is summarized in Figure 4c. For the quantitative data we measured the gas produced by one cell three times consecutively, and here we provide the average data with a confidence interval of 0.95 (see Table S2 for a full dataset). The main components are CO_2 and H_2; there is also a noticeable amount of CO and C_2H_4 as well as admixtures of other hydrocarbons: C_3H_8, C_3H_6, C_2H_6, CH_4. For SIBs, gases after the TR were previously analyzed in Ref.[26] for NVPF-based 18650 cells, where solvent vapors in the gas mixture were also registered.

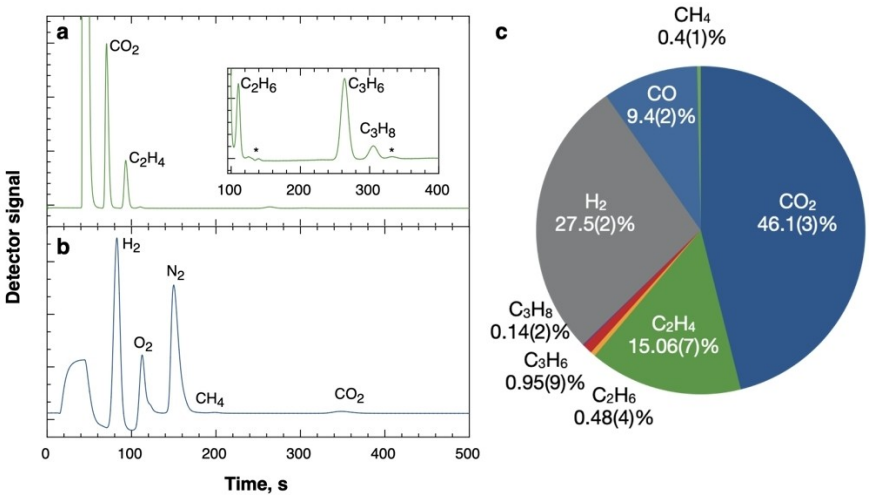

Figure 4. GC results for the Na-ion cell after the thermal runaway measured with a GC-TCD setup with zeolite (5 Å) (a) and Porapak Q sorbent (b) columns. The detected components of the produced gases (mol. %) (c).

Unfortunately, our technique does not allow monitoring the presence of solvent vapors in the gas mixture, however, it provides more accurate quantitative data. Compared to the data obtained in Ref.,[26] we observed higher concentrations of CO_2 and CO relative to H_2. Besides the difference in the cathode battery chemistry, this variance may be due to a more efficient combustion in our experiment, since the highest temperature during thermal acceleration reached 330 °C, while in Ref.[26] for most cells it did not exceed 250 °C.

Generally, the composition of the released gases is similar to that observed for various lithium-ion systems[14,53] since it is mainly determined by the electrolyte, the polymer binder and SEI,[14] all of which are quite similar for both systems.

Conclusions

In summary, we established that $Na_3V_2O_2(PO_4)_2F$-based Na-ion pouch cell undergoes thermal runaway at a relatively high temperature (over 190 °C) under thermal abuse at a 5 °C/min heating rate, which is noticeably higher than for NMC-based LIBs. According to the DSC data, we found that self-heating in this system is mostly related to the anode and separator decomposition; the cathode processes play a minor role. The composition of the gas mixture released during the TR process is close to that for Li-ion batteries since it is mainly determined by the electrolyte, the polymer binder and SEI that are similar for both systems. We believe that this result would be useful for future development of Na-ion batteries with polyanionic compounds.

Acknowledgements

The work was performed under financial support of Russian Science Foundation (project 22–13-00427). The GC measurements were performed using the core research facility of the N.N. Semenov Federal Research Center for Chemical Physics (FRCCP RAS, 506694). The authors acknowledge support from M.V. Lomonosov Moscow State University Program of Development in part of the DSC measurements (DSC 204 HP Phoenix). The authors are grateful to V. Gorshkov for his kind assistance with Na-ion pouch cell preparation and to Dr. M. Sinev for fruitful discussions.

Conflict of Interests

The authors declare no conflict of interest.

Data Availability Statement

The data that support the findings of this study are available from the corresponding author upon reasonable request.

Keywords: Sodium-ion battery · Sodium fluorophosphates · Thermal runaway

[1] G. Zubi, R. Dufo-López, M. Carvalho, G. Pasaoglu, *Renew. Sustain. Energy Rev.* **2018**, *89*, 292–308.
[2] Y. Ding, Z. P. Cano, A. Yu, J. Lu, Z. Chen, *Electrochem. Energy Rev.* **2019**, *2*, 1–28.
[3] P. Jindal, J. Bhattacharya, *J. Electrochem. Soc.* **2019**, *166*, A2165–A2193.
[4] X. Feng, D. Ren, X. He, M. Ouyang, *Joule* **2020**, *4*, 743–770.
[5] S. Mallick, D. Gayen, *J. Energy Storage* **2023**, *62*, 106894.
[6] X. Feng, M. Ouyang, X. Liu, L. Lu, Y. Xia, X. He, *Energy Storage Mater.* **2018**, *10*, 246–267.
[7] Y. Wang, X. Feng, W. Huang, X. He, L. Wang, M. Ouyang, *Adv. Energy Mater.* **2023**, *13*, 2203841.
[8] R. R. Samigullin, O. A. Drozhzhin, E. V. Antipov, *ACS Appl. Energy Mater.* **2022**, *5*, 14–19.
[9] S. K. Martha, O. Haik, E. Zinigrad, I. Exnar, T. Drezen, J. H. Miners, D. Aurbach, *J. Electrochem. Soc.* **2011**, *158*, A1115–A1122.
[10] S.-M. Bak, E. Hu, Y. Zhou, X. Yu, S. D. Senanayake, S.-J. Cho, K.-B. Kim, K. Y. Chung, X.-Q. Yang, K.-W. Nam, *ACS Appl. Mater. Interfaces* **2014**, *6*, 22594–22601.
[11] J. Hou, X. Feng, L. Wang, X. Liu, A. Ohma, L. Lu, D. Ren, W. Huang, Y. Li, M. Yi, Y. Wang, J. Ren, Z. Meng, Z. Chu, G.-L. Xu, K. Amine, X. He, H. Wang, Y. Nitta, M. Ouyang, *Energy Storage Mater.* **2021**, *39*, 395–402.
[12] J. R. Dahn, E. W. Fuller, M. Obrovac, U. von Sacken, *Solid State Ion.* **1994**, *69*, 265–270.
[13] L. Yuan, T. Dubaniewicz, I. Zlochower, R. Thomas, N. Rayyan, *Process Saf. Environ. Prot.* **2020**, *144*, 186–192.
[14] A. W. Golubkov, D. Fuchs, J. Wagner, H. Wiltsche, C. Stangl, G. Fauler, G. Voitic, A. Thaler, V. Hacker, *RSC Adv.* **2013**, *4*, 3633–3642.
[15] A. García, P. Zhao, J. Monsalve-Serrano, D. Villalta, S. Martinez-Boggio, *Appl. Therm. Eng.* **2023**, *218*, 119308.
[16] S. Ohneseit, P. Finster, C. Floras, N. Lubenau, N. Uhlmann, H. J. Seifert, C. Ziebert, *Batteries* **2023**, *9*, 237.
[17] T. Joshi, S. Azam, C. Lopez, S. Kinyon, J. Jeevarajan, *J. Electrochem. Soc.* **2020**, *167*, 140547.
[18] Y.-S. Duh, Y. Sun, X. Lin, J. Zheng, M. Wang, Y. Wang, X. Lin, X. Jiang, Z. Zheng, S. Zheng, G. Yu, *J. Energy Storage* **2021**, *41*, 102888.
[19] J. Lamb, L. Torres-Castro, J. C. Hewson, R. C. Shurtz, Y. Preger, *J. Electrochem. Soc.* **2021**, *168*, 060516.
[20] J. Chen, X. Rui, H. Hsu, L. Lu, C. Zhang, D. Ren, L. Wang, X. He, X. Feng, M. Ouyang, *J. Energy Storage* **2022**, *49*, 104090.
[21] K. Kubota, M. Dahbi, T. Hosaka, S. Kumakura, S. Komaba, *Chem. Rec.* **2018**, *18*, 459–479.
[22] E. Goikolea, V. Palomares, S. Wang, I. R. Larramendi, X. Guo, G. Wang, T. Rojo, *Adv. Energy Mater.* **2020**, *10*, 2002055.
[23] V. Palomares, P. Serras, I. Villaluenga, K. B. Hueso, J. Carretero-González, T. Rojo, *Energy Environ. Sci.* **2012**, *5*, 5884–5901.
[24] K. Chayambuka, G. Mulder, D. L. Danilov, P. H. L. Notten, *Adv. Energy Mater.* **2020**, *10*, 2001310.
[25] X. Zhu, L. Wang, *EcoMat* **2020**, *2*, e12043.
[26] A. Bordes, G. Marlair, A. Zantman, A. Chesnaye, P.-A. L. Lore, A. Lecocq, *ACS Energy Lett.* **2022**, *7*, 3386–3391.
[27] J. B. Robinson, T. M. M. Heenan, J. R. Jervis, C. Tan, E. Kendrick, D. J. L. Brett, P. R. Shearing, *J. Power Sources* **2018**, *400*, 360–368.
[28] G. Cui, H. Wang, F. Yu, H. Che, X. Liao, L. Li, W. Yang, Z. Ma, *Chin. J. Chem. Eng.* **2022**, *46*, 280–286.
[29] J. Robinson, D. Finegan, T. Heenan, K. Smith, E. Kendrick, D. Brett, P. R. Shearing, *J. Electrochem. Energy Convers. Storage* **2017**, *15*, 011010.
[30] Y. Li, Y.-S. Hu, X. Qi, X. Rong, H. Li, X. Huang, L. Chen, *Energy Storage Mater.* **2016**, *5*, 191–197.
[31] M. He, A. E. L. Mejdoubi, D. Chartouni, M. Morcrette, P. Troendle, R. Castiglioni, *J. Power Sources* **2023**, *588*, 233741.
[32] Q. Zhou, Y. Li, F. Tang, K. Li, X. Rong, Y. Lu, L. Chen, Y.-S. Hu, *Chin. Phys. Lett.* **2021**, *38*, 076501.
[33] Z. Li, M. Dadsetan, J. Gao, S. Zhang, L. Cai, A. Naseri, M. E. Jimenez-Castaneda, T. Filley, J. T. Miller, M. J. Thomson, V. G. Pol, *Adv. Energy Mater.* **2021**, *11*, 2101764.
[34] Y. Zheng, Z. Shi, D. Ren, J. Chen, X. Liu, X. Feng, L. Wang, X. Han, L. Lu, X. He, M. Ouyang, *J. Energy Chem.* **2022**, *69*, 593–600.
[35] M. P. Do, P. J. Fischer, A. Nagasubramanian, J. Geder, F. E. Kühn, M. Srinivasan, *J. Electrochem. Soc.* **2019**, *166*, A944–A952.
[36] I. U. Mohsin, C. Ziebert, M. Rohde, H. J. Seifert, *J. Electrochem. Soc.* **2021**, *168*, 050544.

[37] L. Sharma, S. P. Adiga, H. N. Alshareef, P. Barpanda, *Adv. Energy Mater.* **2020**, *10*, 2001449.
[38] Z. Hao, X. Shi, Z. Yang, X. Zhou, L. Li, C. Ma, S. Chou, *Adv. Mater.* **2024**, *36*, e2305135.
[39] G. P. Lakienko, Z. V. Bobyleva, V. S. Gorshkov, A. I. Zybina, O. A. Drozhzhin, A. M. Abakumov, E. V. Antipov, *J. Electrochem. Soc.* **2024**, *171*, 060512.
[40] D. Burova, I. Shakhova, P. Morozova, A. Iarchuk, O. A. Drozhzhin, M. G. Rozova, S. Praneetha, V. Murugan, J.-M. Tarascon, A. M. Abakumov, *RSC Adv.* **2019**, *9*, 19429–19440.
[41] Y. Pan, Y. Zhang, B. S. Parimalam, C. C. Nguyen, G. Wang, B. L. Lucht, *J. Electroanal. Chem.* **2017**, *799*, 181–186.
[42] J. Fondard, E. Irisarri, C. Courrèges, M. R. Palacin, A. Ponrouch, R. Dedryvère, *J. Electrochem. Soc.* **2020**, *167*, 070526.
[43] A. Ponrouch, E. Marchante, M. Courty, J.-M. Tarascon, M. R. Palacín, *Energy Environ. Sci.* **2012**, *5*, 8572–8583.
[44] K. Mukai, T. Inoue, *Electrochem. Commun.* **2018**, *88*, 101–104.
[45] M. Palanisamy, K.-W. Lin, C.-T. Lo, V. G. Pol, *ACS Appl. Mater. Interfaces* **2022**, *14*, 28310–28320.
[46] M. M. Rahman, S. Mateti, Q. Cai, I. Sultana, Y. Fan, X. Wang, C. Hou, Y. Chen, *Energy Storage Mater.* **2019**, *19*, 352–359.
[47] Y. S. Chung, S. H. Yoo, C. K. Kim, *Ind. Eng. Chem. Res.* **2009**, *48*, 4346–4351.
[48] X. Gao, W. Sheng, Y. Wang, Y. Lin, Y. Luo, B. Li, *J. Appl. Polym. Sci.* **2015**, *132*, 42169.
[49] X. Chen, C. Liu, Y. Fang, X. Ai, F. Zhong, H. Yang, Y. Cao, *Carbon Energy* **2022**, *4*, 1133–1150.
[50] A. Kvasha, C. Gutiérrez, U. Osa, I. de Meatza, J. A. Blazquez, H. Macicior, I. Urdampilleta, *Energy* **2018**, *159*, 547–557.
[51] C. Pablos, J. Olchowka, E. Petit, G. Minart, M. Duttine, F. Weill, C. Masquelier, D. Carlier, L. Croguennec, *Chem. Mater.* **2023**, *35*, 4078–4088.
[52] N. N. Semenov, *Usp. Fiz. Nauk* **1940**, *23*, 251–292.
[53] Y. Fernandes, A. Bry, S. de Persis, *J. Power Sources* **2018**, *389*, 106–119.

Manuscript received: June 14, 2024
Revised manuscript received: September 9, 2024
Accepted manuscript online: October 14, 2024
Version of record online: November 12, 2024